ELSEVIER

Biophysical Chemistry 104 (2003) 259–270

Biophysical Chemistry

www.elsevier.com/locate/bpc

Physico-chemical studies of a DNA triplex containing a new ferrocenemethyl-thymidine residue in the third strand

L. Petraccone[a], E. Erra[a], A. Messere[b], D. Montesarchio[c], G. Piccialli[d], G. Barone[a], C. Giancola[a,*]

[a]*Dipartimento di Chimica, Università 'Federico II' di Napoli, Via Cintia 4, 80126, Napoli, Italy*
[b]*Dipartimento di Scienze Ambientali, Seconda Università di Napoli, 81100, Caserta, Italy*
[c]*Dipartimento di Chimica Organica e Biochimica, Università 'Federico II' di Napoli, Via Cintia 4, 80126, Napoli, Italy*
[d]*Dipartimento di Chimica delle Sostanze Naturali, Via D. Montesano 49, 80131 Napoli, Italy*

Received 4 October 2002; received in revised form 18 November 2002; accepted 19 November 2002

Abstract

The stability of a 16-mer DNA triple helix containing a 3-*N*(ferrocenemethyl)-thymidine residue in the third strand has been investigated in comparison with the unmodified triplex of the same sequence. A complete physico-chemical characterization of the two triple helices on changing the pH by means of calorimetry, circular dichroism and molecular modeling is therefore reported. The thermodynamic parameters were obtained in the pH range 5.5–7.2 by differential scanning calorimetry (DSC). For both triplexes the T_m and ΔH° (T_m) values increase on decreasing the pH. In the pH range 7.2–6.0 the triplex containing the ferrocenemethyl nucleoside is less stable than the unmodified one, whereas the modified triplex becomes more stable at pH 5.5. Such difference in stability at each pH value is overwhelmingly enthalpic in origin. CD spectra show conformational changes on decreasing the pH for both the triplexes. By spectroscopic pH titration the apparent pK_a values of the cytosines in the two triplexes could be estimated, with the cytosines in the TFO containing the ferrocenemethyl residue having lower apparent pK_a values. These results are consistent with the calorimetric data, showing a decrease of the thermodynamic parameters in the pH range 7.2–6.0 and an increase at pH 5.5 for the ferrocenylated triplex with respect to the unmodified one. The thermodynamic and spectroscopic data are also discussed in relation to molecular models.

Keywords: DNA triple helix; Differential scanning calorimetry; Circular dichroism; Thermodynamic stability; Molecular mechanics

1. Introduction

Triplex forming oligonucleotides (TFOs) specifically bind to duplex DNA and offer a strategy for site-directed gene regulation in eukaryotes [1]. TFOs can be used to introduce site-specific genome modification, to prevent transcription or to inhibit virus propagation [2–4]. Selective and efficient recognition of DNA by TFOs occurs by specific hydrogen bonding formation between the TFO bases and the purines in the major groove of the target DNA double helix [5]. A homopyrimidine third strand binds parallel to the purine strand of the double-stranded target forming T–A·T and C–G·C^+ triplets via Hoogsteen hydrogen bonding,

*Corresponding author. Tel.: +39-081-674266; fax: +39-081-674090.
E-mail address: giancola@chemistry.unina.it (C. Giancola).

0301-4622/03/$ - see front matter © 2003 Elsevier Science B.V. All rights reserved.
PII: S0301-4622(02)00380-0

whereas a purine third strand binds in an antiparallel orientation forming T–A·A and C–G·G base triplets via reverse Hoogsteen hydrogen bonding. The affinity and specificity of third strand binding are affected by a number of factors, such as sequence length, composition, and the presence of modified nucleotides, as well as solution conditions, including pH and mono and divalent counterions concentration [6,7] Physico-chemical studies are essential to determine and, if possible, predict the effects that these factors have on the stability of DNA triplexes.

Recently, several nucleobases and nucleosides functionalized with ferrocene derivatives have been synthesized in an effort to explore their therapeutic potential [8]. In fact, iron-containing sandwich compounds are known to display a pronounced anti-tumoral activity [9], with localization of the metal-bound species in the cell nucleus. The biological activity of ferrocenyl derivatives is thought to involve non-covalent interactions with nucleic acids, which is of great interest in the systematic design of non-platinum group metal antitumor drugs [10,11]. In addition, it has been shown that ferrocene moieties can be useful electrochemical probes and, covalently bound to the 5′-end of oligodeoxyribonucleotides (ODNs), can be exploited as extremely sensitive markers to detect specific DNA and RNA targets, even in very complex mixtures, as an alternative to hazardous and short-living radioisotopes [12,13].

Some of us recently reported a simple and efficient synthetic method to produce ODNs containing a ferrocenemethyl residue at any defined position of the chosen sequence [14]. This target has been achieved by synthesizing the new 3-N(ferrocenemethyl)thymidine nucleoside (**T***, Fig. 1), inserted in internal positions of ODN chains by standard solid phase phosphoramidite protocols. The synthesized modified oligomers have been studied in their ability to form duplex and triplex structures with complementary sequences by UV melting and CD analysis. The presence of the ferrocene group at the 3-N position, as expected, seriously affected the binding process with complementary single strand ODNs, destabilizing the double helical complexes. On the other hand, more

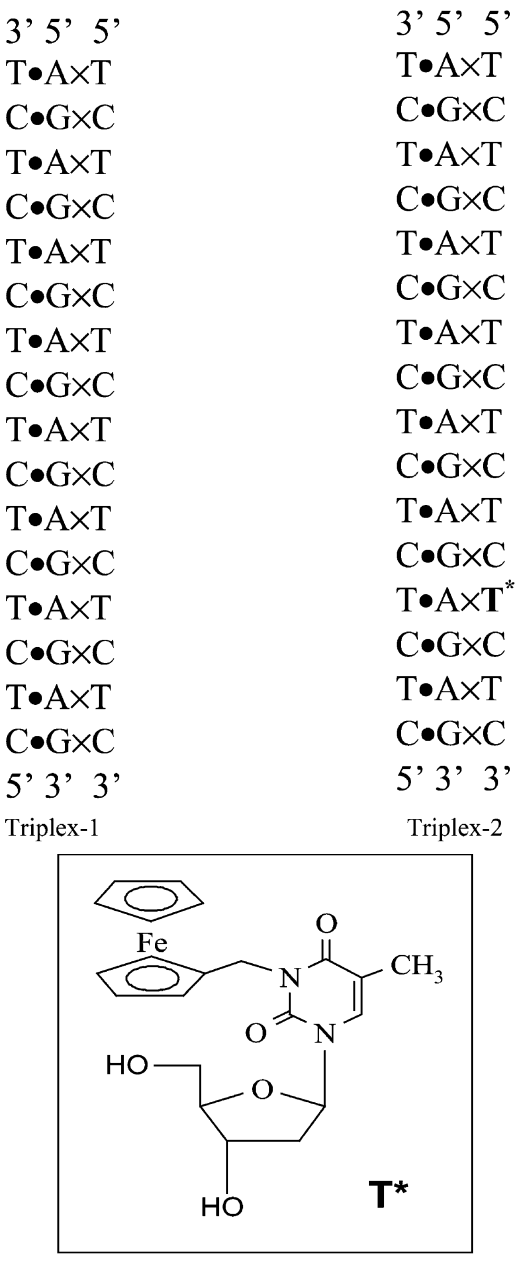

Fig. 1. Schematic representation of the 16-mer triplex (triplex-1), the 16-mer modified triplex (triplex-2), and the ferrocenemethyl-thymidine (T*).

intriguing were the hybridization properties of ferrocene-containing TFOs, which showed a decreased affinity towards the target duplex at

neutral and lightly acidic pH, while at pH 5.5 exhibited sensibly higher T_m values for the triplex dissociation process, with respect to the same unmodified third strand.

In an effort to clarify this behavior and to better characterize these triplex structures, in this work we compare the thermodynamic stability of the two triple helices formed by targeting the same 16-mer duplex with either $^{5'}$TCTCTCTCTCTCT-CTC$^{3'}$ (the corresponding triplex was named triplex-1), or $^{5'}$TCTCTCTCTCTC**T***CTC$^{3'}$ (the corresponding triplex was named triplex-2, see Fig. 1). Differential scanning calorimetry was used to characterize the thermodynamics of formation of the two triplexes. Circular dichroism spectra were performed to evidence conformational differences between the two triplexes. Molecular modeling study was used to highlight the main structural features in the proximity of the ferrocenemethyl-thymidine residue.

2. Materials and methods

2.1. Oligonucleotides

All the oligonucleotides were synthesized on a Millipore Cyclone Plus automated DNA synthesizer following standard phosphoramidite procedures [15,16]. The ferrocenemethyl-thymidine nucleotide was synthesized via a Mitsunobu reaction [17] of ferrocenemethanol with a sugar protected thymidine, then converted into the corresponding 3′-phosphoramidite and incorporated into the desired ODN chain as previously reported [14]. Purification of the modified and natural oligomers was carried out by HPLC on an analytical anion exchange column (Partisil 10 SAX Whatman, 4.6×250 mm, 7 μm). The isolated compounds were then characterized by MALDI-TOF spectrometry. The triplexes were formed by mixing stoichiometric amounts of the three oligonucleotides in the appropriate buffer and heating the solution to 90 °C for 5 min. The solution was slowly cooled to room temperature, then equilibrated for 24 h at 4 °C before performing DSC and CD experiments. The buffer used was 140 mM KCl, 5 mM NaH_2PO_4, 5 mM $MgCl_2$. Potassium chloride (Sigma), monosodium phosphate (Sigma) and magnesium chloride (Carlo Erba) were used as obtained from commercial suppliers. The solutions were adjusted to desired pH values with 1 M HCl or 1 M NaOH. The pH of solutions was measured using a Radiometer pHmeter model PHM 93 at 25 °C. The ODN concentrations were determined spectrophotometrically at 260 nm, using the following extinction coefficients calculated by a nearest neighbor model [18]: 122 000 M^{-1} cm^{-1} for $^{5'}$TCTCTCTCTCTCTCTC$^{3'}$ and $^{5'}$TCTCTCTCTCTCT*CTC$^{3'}$; 188 000 M^{-1} cm^{-1} for $^{5'}$AGAGAGAGAGAGAGAG$^{3'}$; 123 000 M^{-1} cm^{-1} for $^{3'}$TCTCTCTCTCTCTCTC$^{5'}$.

2.2. Differential scanning calorimetry

DSC measurements were performed on a second generation Setaram Micro-DSC at the scan rate of 0.5 °C/min. The calorimetric unit was interfaced to an IBM PC computer for automatic data collection and analysis using the software previously described [19]. The apparent molar heat capacity vs. temperature profiles were obtained by subtracting buffer vs. buffer curves from the sample vs. buffer curves. The data were normalized with regard to the concentration, sample volume and scan rate and are reported in Fig. 2. The excess heat capacity function $\langle C_p \rangle$ was obtained after baseline subtraction, assuming that the baseline is given by the linear temperature dependence of the native state heat capacity [20]. The reversibility of the thermal processes was verified by checking the reproducibility of the calorimetric trace in a second heating of the samples immediately after cooling from the first scan.

The process enthalpies for the double helix alone, ΔH° (T_m), were obtained by integrating the area under the heat capacity vs. temperature curves. T_m is the temperature corresponding to the maximum of each DSC peak. The entropy changes for the double helix alone, ΔS° (T_m), were determined by integrating the curve obtained by dividing the heat capacity curve by the absolute temperature. van't Hoff values were obtained by DSC profiles utilizing the equation:

$$\Delta H^\circ_{v.H.} = 6RT_m^2 \Delta C_p^\circ(T_m)/\Delta H^\circ(T_m) \quad (1)$$

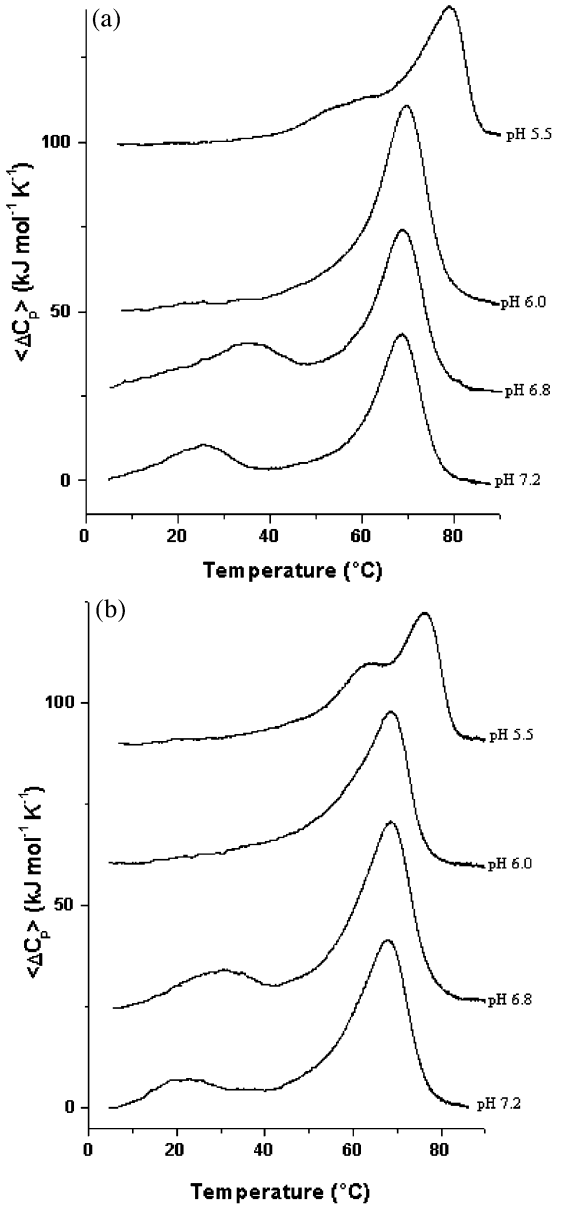

Fig. 2. Calorimetric heat capacity vs. temperature profiles at pH 7.2, 6.8, 6.0 and 5.5 for the triplex-1 (panel a) and triplex-2 (panel b). Excess capacity values have been shifted along the *y*-axis for ease of presentation.

where T_m is the maximum of the DSC peak, $\Delta C_p^{\circ}(T_m)$ is the value of the excess heat capacity function at T_m, ΔH° (T_m) is the calorimetric enthalpy directly obtained by the area under the DSC peak and the number 6 originates from the stoichiometry of the reaction.

The calorimetric melting profiles of the triple helices were modeled by two sequential bimolecular transitions:

$$\mathrm{ABC} \overset{K_1}{\leftrightarrow} \mathrm{A} + \mathrm{BC} \overset{K_2}{\leftrightarrow} \mathrm{A} + \mathrm{B} + \mathrm{C}$$

where ABC indicates the triple helix, BC the target duplex and A the TFO.

Considering the stoichiometry and conservation of mass the following equations hold at any temperature:

$$C_t = C_{\mathrm{ABC}} + C_{\mathrm{BC}} + C_{\mathrm{B}} \tag{2}$$

$$C_t = C_{\mathrm{ABC}} + C_{\mathrm{A}} \tag{3}$$

$$C_{\mathrm{A}} = C_{\mathrm{B}} + C_{\mathrm{BC}} \tag{4}$$

$$C_{\mathrm{C}} = C_{\mathrm{B}} \tag{5}$$

where C_t, the molar concentration of the third strand, corresponds to the concentration of the double helix and, at low temperature, of the triple helix too.

The fractional population of each species can be defined as:

$$f_x = \frac{C_x}{C_t} \tag{6}$$

where x represents ABC, BC and A and the above equations can be rewritten as:

$$f_{\mathrm{ABC}} + f_{\mathrm{BC}} + f_{\mathrm{B}} = 1 \tag{7}$$

$$f_{\mathrm{ABC}} + f_{\mathrm{A}} = 1 \tag{8}$$

$$f_{\mathrm{A}} = f_{\mathrm{B}} + f_{\mathrm{BC}} \tag{9}$$

$$f_C = f_B \quad (10)$$

The two equilibrium constants, K_1 and K_2, are:

$$K_1 = \frac{f_A f_{BC}}{f_{ABC}} C_t \quad (11)$$

$$K_2 = \frac{f_B f_C}{f_{BC}} C_t \quad (12)$$

Combining the above relations the following coupled non-linear equations are obtained:

$$f_A = \frac{1 - f_A}{f_{BC}} \frac{K_1}{C_t} \quad (13)$$

$$f_{BC} = (f_A - f_{BC})^2 \frac{C_t}{K_2} \quad (14)$$

Eqs. (7)–(10) along with Eqs. (13) and (14) completely describe the set of sequential reactions. Their solution permits the determination of the excess enthalpy $\langle \Delta H \rangle$ of this system according to the equation:

$$\langle \Delta H \rangle = f_A \Delta H_1 + f_B \Delta H_2 \quad (15)$$

where ΔH_1 and ΔH_2 are the enthalpy changes of the two sequential transitions.

The corresponding excess heat capacity, $\langle \Delta C_p \rangle$, can be calculated through numerical differentiation of Eq. (15):

$$\langle \Delta C_p \rangle = \frac{\partial \langle \Delta H \rangle}{\partial T} \quad (16)$$

At any temperature the equilibrium constants have been determined according to the equation:

$$K_i = K_i(T_{mi}) e^{\left(-\frac{\Delta H_i}{R}\right)\left(\frac{1}{T} - \frac{1}{T_{mi}}\right)} \quad (17)$$

where we assumed that T_{mi} is the temperature at which K_i is equal to $C_t/2$.

Table 1
T_m, enthalpy and entropy parameters for ABC ↔ A + BC transitions[a]

Triplex	pH	T_m (°C)	$\Delta H°$ (T_m) (kJ mol^{-1})	$\Delta S°$ (T_m) (kJ mol^{-1} K^{-1})
Triplex-1				
	7.2	25.2	130 ± 13	0.48 ± 0.06
	6.8	34.0	190 ± 10	0.64 ± 0.04
	6.0	58.5	255 ± 7	0.78 ± 0.02
	5.5	59.0	256 ± 7	0.80 ± 0.03
Triplex-2				
	7.2	20.0	82 ± 10	0.31 ± 0.04
	6.8	28.5	103 ± 11	0.38 ± 0.05
	6.0	53.0	230 ± 8	0.74 ± 0.03
	5.5	61.0	295 ± 10	0.91 ± 0.04

[a] For BC ↔ B + C transition the thermodynamic parameters at pH 7.2, 6.8 and 6.0 for both the triplexes are: T_m = 69.0 °C, $\Delta H°$ (T_m) = 480 ± 16 kJ mol^{-1} and $\Delta S°$ (T_m) = 1.40 ± 0.05 kJ mol^{-1} K^{-1}. At pH 5.5 for the same transition the thermodynamic parameters are: T_m = 77.0 °C, $\Delta H°$ (T_m) = 480 ± 16 kJ mol^{-1} and $\Delta S°$ (T_m) = 1.37 ± 0.05 kJ mol^{-1} K^{-1}.

We solved Eqs. (13) and (14) numerically for the fractional populations and subsequently we determined the heat capacity through numerical differentiation of Eq. (15), using a self-made MATHLAB program and assuming that the ΔH_i values were constant. T_m and ΔH_i values reported in Table 1 for pH 5.5 and 6.0 provide the best fit of the experimental triplex denaturation curves. The global simulated excess heat capacity curves were split in the two corresponding subtransitions defined by:

$$\langle \Delta C_{p,i} \rangle = \Delta H_i \frac{\partial f_i}{\partial T} \quad (18)$$

where f_i is f_B or f_A (see Eq. (15)).

The ΔS_i° values were calculated integrating curves obtained by dividing the two simulated subtransitions curves by the absolute temperatures, i.e. $\Delta S_i^0 = \int \left(\langle \Delta C_{p,i} \rangle / T \right) dT$.

The errors in T_m do not exceed 0.2 °C and the errors for $\Delta H°$ (T_m) and $\Delta S°$ (T_m) are the standard deviations of the mean from the multiple measurements.

2.3. CD measurements

CD spectra were obtained on a JASCO 715 circular dichroism spectrophotometer at 5 °C in a 0.1 cm pathlength cuvette. The wavelength was varied from 200 to 340 nm at 5 nm min^{-1}. CD spectra were recorded with a response of 16 s, at 2.0 nm bandwidth and normalized by subtraction of the background scan with buffer. pH titrations were accomplished by addition of microliter amounts of 1 M HCl to the solution containing the triplex. The molar ellipticity was calculated from the equation $[\vartheta]=\vartheta/cl$ where ϑ is the relative intensity, c the concentration of the triplex and l is the pathlength of the cell in cm. The points reported in the sigmoidal curves derive from respective spectra, which are an average of at least three scans. The sigmoidal curves were obtained using the Boltzman fit of Origin program. The error on the inflection point is $<1\%$.

Temperature was kept constant with a thermoelectrically controlled cell holder (JASCO PTC-348).

2.4. Molecular modeling

Investigation of the conformation of the two triplexes has been performed by means of molecular mechanics calculations. Models of the two triplexes were built from the helical coordinates given by Liu, who reported a B-like conformation for the duplex portion in a triplex [21]. The ferrocene of the ferrocenemethyl-thymidine was constructed in a staggered configuration and a ZINDO/1 semi-empirical method was used to optimize the geometry and to determine the partial charges for the atoms [22,23].

The two triplexes were neutralized by adding 45 sodium counterions. Each Na^+ counterions was placed on the phosphate bisector 3 Å from the P atom and then each triplex was individually placed in a 35.1 Å×35.1 Å×56.1-Å box of Monte Carlo TIP3P water, with periodic boundary conditions [24]. Water molecules closer than 2.3 Å from the solute atoms were removed. The final system contained 1562 solute atoms and 1632 water molecules in the case of triplex-1, and 1573 solute atoms and 1627 water molecules in the case of triplex-2. For both triplexes the same energy minimization procedure was used.

The Amber force field [25] was used. The nonbonded interactions were cut-off using a switching function at 16.0 Å. The hydrogen bonds of the two terminal base triplets were strengthened with a harmonic potential to avoid end-fraying effects. The force constant was set to 50 kcal mol^{-1} $Å^{-2}$ and the equilibrium hydrogen bond length to 2.5 Å. Starting structures were minimized using 1500 steps of the steepest descent method followed by the conjugate method until convergence to a r.m.s. gradient of 0.1 kcal mol^{-1} $Å^{-1}$.

3. Results

3.1. Thermodynamics of triplex formation

The thermal stability of the two triple helices was studied decreasing the pH from 7.2 to 5.5, keeping the concentration constant at 4.4×10^{-4} M. The calorimetric profiles are shown in Fig. 2. At pH 7.2 and 6.8, the two transitions are well resolved: the first low-temperature transition is attributable to the release of the third strand from the target double helix, and the second transition at higher temperature is relative to the dissociation of the double helix. In fact, the latter transition under comparable conditions, coincides with the melting transition of the free double helix.

The melting of the triplexes is strongly dependent on pH, according to the presence of cytosines in the TFO strand [26–28], whereas the thermal stability of the duplex is not influenced by pH in the range 6.0–7.2. Nevertheless, at pH 5.5 the T_m for the duplex dissociation is 8 °C higher, reflecting a pH influence. It is reported that at low pH the protonation of the duplex bases, especially of cytosines, contributes to the stabilization of the double helix by hydrogen bonding and electrostatic interactions of protonated groups with the nearby phosphate residues [29].

Since on decreasing the pH the triplex–duplex transition is shifted to higher temperatures, the two transitions are not well separated, then the deconvolution procedure was used to obtain the two corresponding subtransition curves (see Section 2). Fig. 3 shows good agreement between the

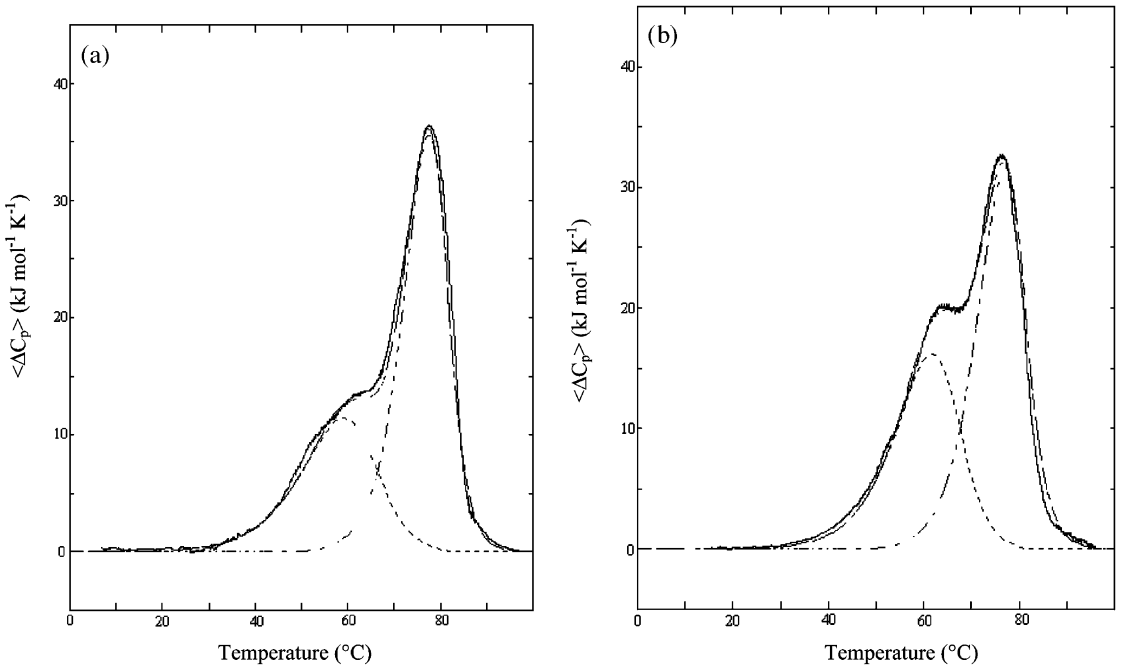

Fig. 3. Excess heat capacity of triplex-1 (Panel a) and triplex-2 (Panel b) at pH 5.5, experimental data (solid line), total simulated transition (dotted line) and deconvolution in two transitions (dashed line and dashdot line).

experimental calorimetric curve and the simulated one for triplex-1 and triplex-2 at pH 5.5. Similar agreement has been found for both triplexes at pH 6.0. Thermodynamic parameters of the two triplexes at each of the pH values are listed in Table 1. The values reported for pH 5.5 and 6.0 derive from deconvolution procedure. The main issues are: (i) for both the triplexes the T_m and ΔH° (T_m) values increase on decreasing the pH; (ii) triplex-2 is less stable than triplex-1 in the pH range 7.2–6.0, but is more stable at pH = 5.5; (iii) the difference in stability is overwhelmingly enthalpic in origin.

In more detail, the ΔH° values for triplex-1 (ferrocene-free) are systematically lower than the corresponding values for triplex-2 except at pH 5.5, where triplex-2 is enthalpically more stable by 39 kJ mol^{-1}. The same trend is observed for the T_m values: in the pH range 7.2–6.0, triplex-2 is thermally less stable (ΔT_m, −5.5 °C), whereas at pH 5.5 triplex-2 shows $\Delta T_m = +2$ °C with respect to triplex-1. Fig. 3 shows that at pH 5.5 the peak at lower temperature, relative to triplex–duplex dissociation, is centered at 59 °C for the unmodified triplex and at 61 °C for the modified triplex, whereas the peak at higher temperature, due to duplex dissociation, remains at 77 °C for both the triplexes. Van't Hoff enthalpy calculated by means of Eq. (1) gives a value of 480 kJ mol^{-1} for the duplex dissociation, in good agreement with the calorimetric values and the expected value calculated by the Santalucia method [30]. For the triplex to duplex dissociation the van't Hoff enthalpy is 260 kJ mol^{-1} that agrees well with the calorimetric enthalpies obtained at pH 6.0 and 5.5.

In the pH range 6.0–7.2 the change in entropy for triplex-2 formation is less unfavorable than in the case of triplex-1, so most of the thermal stability of the latter is attributable to the enthalpic term. The same considerations on the entropy contribution can be extended to pH 5.5. At this pH value, the major thermodynamic stability of triplex-2 is still enthalpic in origin.

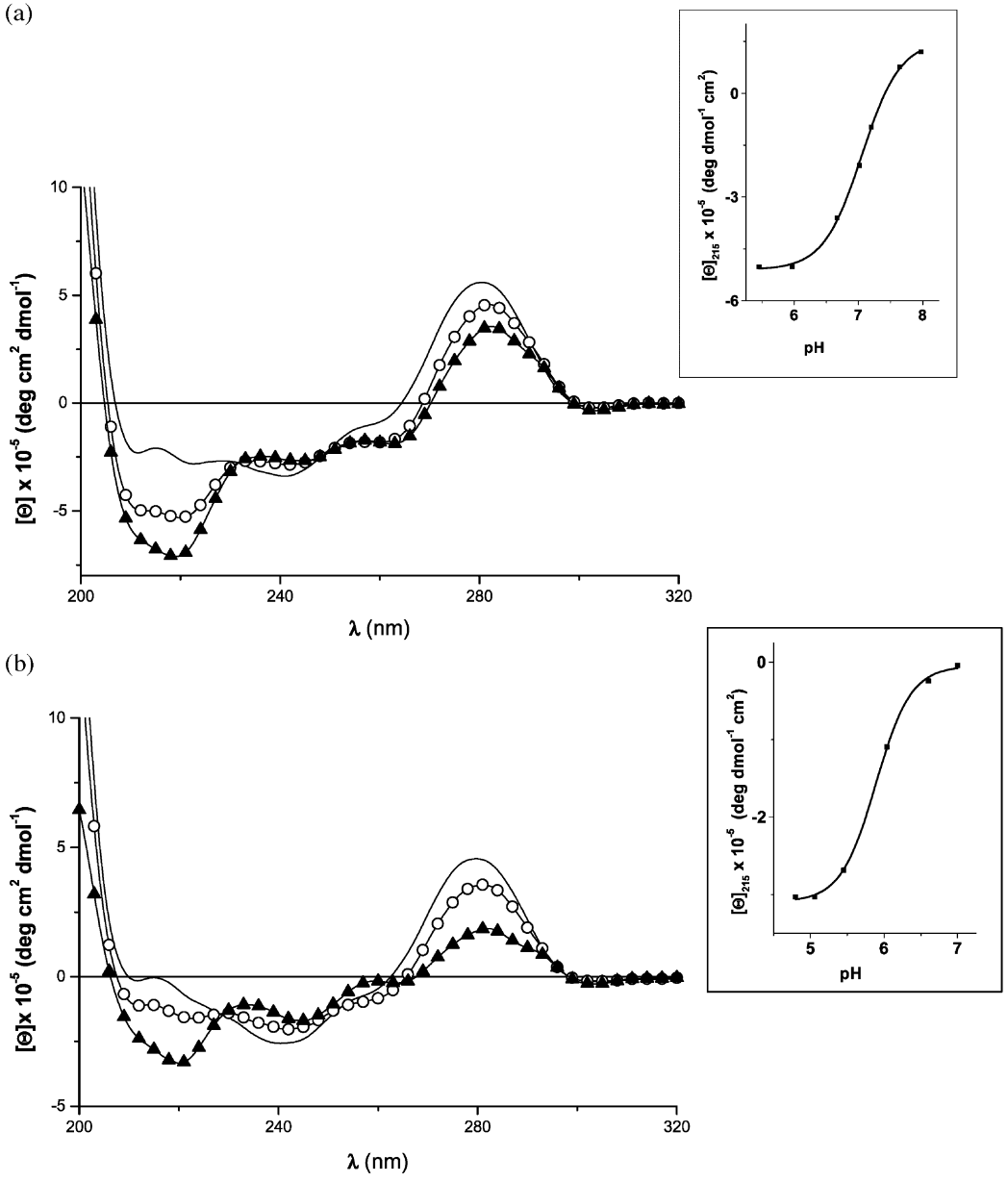

Fig. 4. CD spectra of the triplex-1 (panel a) and triplex-2 (panel b) as a function of pH: pH 7.0 (solid line); pH 6.0 (○) and pH 5.0 (▲). The inserts show the variation of molar ellipticity at 215 nm as a function of pH.

3.2. Circular dichroism at different pH values

Circular dichroism spectra of the triplexes as a function of pH are displayed in Fig. 4. At pH 5.5, the CD spectrum is characterized by a large positive band at 276 nm and a negative band at 215 nm. Significantly, the negative band at 215 nm is indicative of the existence of triple-stranded DNA [31]. As the pH is increased, the negative band at 215 nm is reduced in magnitude and shifted to

lower wavelength, while the positive band at 276 nm is slightly increased in magnitude and shifted to lower wavelength. We found a similar behavior for both the triplexes. These results are consistent with a pH-induced transition relative to the dissociation of the third strand from the target double helix. Fig. 4 (inserts) shows the pH dependence of the molar ellipticity at 215 nm for triplex-1 and triplex-2, respectively. Inspection of the obtained curves reveals the apparent pK_a of the pH-induced transition of the triplexes to be approximately 7 for triplex-1 and 6 for triplex-2.

3.3. Modeling studies

In order to gain information on the molecular geometry of the two triple helices, especially in the modified residue region of triplex-2, molecular mechanics calculations were performed. The energy minimization was carried out with inclusion of explicit water, counterions and using a unitary dielectric constant. The molecular models of both triplexes are shown in Fig. 5. The integrity of the two triplexes is maintained after minimization and all the bases of the third strands form the Hoogsteen H-bonds, except the modified base in triplex-2. Indeed, analyzing the ferrocenemethyl-thymidine region in triplex-2, it can be noted that the thymine bearing a ferrocenemethyl residue at N-3 position points outwards with respect to the duplex major groove and does not participate in Hoogsteen hydrogen bonds. This displacement of the thymine base from its natural position in the unmodified triplet TxA·T (as in the case of triplex-1) causes the exposure to the solvent of the cytosines directly bonded to the modified residue *T**. However, the model suggests that the ferrocenemethyl residue is able to adapt its geometry to the duplex major groove without causing further distortions of the global geometry of the triplex and duplex. Furthermore, the interatomic distances between the ferrocene aromatic rings atoms and the duplex major groove hydrogen bonding sites suggest the possibility of favorable non-bonded interactions.

4. Discussion

The comparison between the CD spectra of two triplexes (Fig. 4a,b) indicates that the ferrocenemethyl-thymidine nucleoside does not disrupt the global geometry of the triplex but lowers the apparent pK_a value relative to N^3-cytosine residues protonation. The effects of pH on the molar ellipticity at 215 nm and 5 °C are shown as inserts in Fig. 4a for triplex-1 and in Fig. 4b for triplex-2. The inflection point is pH 7.0 for triplex-1 and pH 6.0 for triplex-2. It should be considered that the pK_a value of cytosines involved in Hoogsteen bonds can be some units above 4.3, which is the reported value for the free cytosine residue [28]. However, as recent NMR studies on an intramolecular triple helix have shown, protonation strongly depends on the cytosine position within a particular triple helix and it can be very different for several third strand sequences [32,33]. For example, values of 9.0 and 6.0 were reported for internal and terminal cytosine residues in the third strand, respectively [34]; this difference is clearly related to a minor or major exposure to the solvent depending on the location of the cytosine residue within the chain. In the present case, it is possible that the observed decrease in pH-induced stabilization for triplex-2 with respect to triplex-1 may arise from a local influence of the ferrocenemethyl-thymidine on pK_a values of the two cytosines directly linked to the modified residue. Molecular models of the two triplexes, obtained by molecular mechanics calculations, reinforce this hypothesis. Analyzing the ferrocenemethyl-thymidine region (Fig. 5), it can be noted that the plane of the modified thymine is completely thrown out from its natural position, owing to steric hindrance of the ferrocene moiety. This conformational change allows the creation of a cavity, accessible to the solvent which probably favors deprotonation of the cytosines and consequently, Hoogsteen H-bonds destruction in the pH range 6.0–7.2. Hence, the observed decrease in stability of triplex-2 in this pH range may be due to the bulge induced by the presence of ferrocene moiety at *T**, which not only disrupts one TxA·T triplet, but also causes a higher exposure to the solvent of the adjacent cytosines in the third strand. In addition, the interactions of these cytosines with only one triplet-structured nearest-neighbor induce a lower stabilization than in a completely stacked structure, where each can interact with two fully-structured

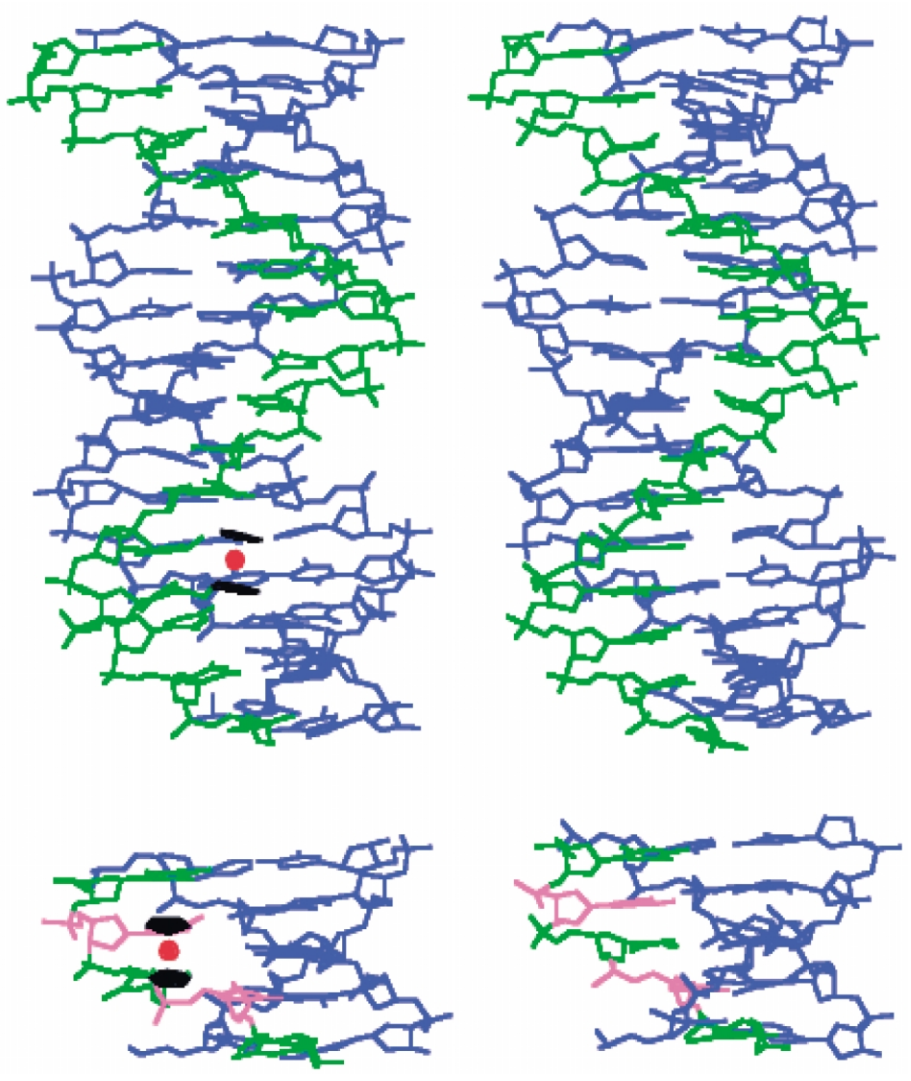

Fig. 5. Molecular models of the triplex-1 (on the right) and the triplex-2. The Watson–Crick strands are shown in blue and the third strands are shown in green. For clarity, at the bottom, the corresponding ferrocenemethyl-thymidine regions are also reported in another perspective. The ferrocene residue is shown in black and red (Fe-atom). The cytosines linked to the modified residue are shown in violet.

nearest neighbors. This could justify the penalty in enthalpy for the triplex-to-duplex transition of triplex-2 with respect to triplex-1 in the pH range 7.2–6.0. The $\Delta\Delta H^\circ$ is 60 kJ mol^{-1} at pH 7.2, 90 kJ mol^{-1} at pH 6.8 and 25 kJ mol^{-1} at pH 6.0. Furthermore, DSC data also show that the T_m values for triplex-2 are always lower than the corresponding values for triplex-1 in the same pH range. On the other hand, at pH 5.5 the ΔH° and T_m of triplex-2 dissociation are higher than those of triplex-1. ΔG° values calculated at 298 K, at this pH, for the dissociation of TFO from the target duplex are 17.6 kJ mol^{-1} and 23.8 kJ mol^{-1} for triplex-1 and triplex-2, respectively, i.e. the triplex containing the ferrocene residue is 6.2 kJ mol^{-1} more stable.

These findings indicate that one ferrocenyl group linked to the 3-N position of a thymine residue in an oligopyrimidine TFO affects the triple helix for at least two contrasting factors. The first one is the previously discussed influence of the ferrocene residue on the effective pK_a value of the cytosines of the third strand, the second one is the favorable interactions between ferrocene and DNA bases, also described by Ihara et al. [35]. They indicate some synergistic effects as the additional hydrogen bonds and the hydrophobic interactions between the modified TFO and the base pairs in duplex major groove. These favorable interactions probably become much more effective once a complete protonation of the two cytosines adjacent to the modified thymine occurs ($pH < 6$). The protonated cytosine with its Hoogsteen bonds, in fact, could contribute to keeping the ferrocene residue in the major groove of the double helix. Hence, in the pH range 7.2–6.0 the destabilizing effect due to the deprotonated cytosines is the prevailing one and overwhelms the favorable triplex–ferrocene interactions, whereas at pH 5.5 the favorable hydrophobic interactions are predominant because all the cytosines are protonated.

In conclusion, the present physico-chemical study confirms that ferrocene-containing oligonucleotides can be included in the repertoire of useful TFOs, since they give origin to sufficiently stable triplexes and therefore can be exploited in a variety of DNA-directed applications, either as an electrochemical probe or for pharmaceutical purposes. However, solution conditions, and especially pH conditions, play a crucial role in the stabilization of the triple helical structure, and therefore have to be strictly under control to avoid undesired secondary effects.

Acknowledgments

This work was supported by a PRIN-MURST grant from the Italian 'Ministero dell'Università e della Ricerca Scientifica e Tecnologica' (Rome).

References

[1] M.S. Searle, NMR studies of drug–DNA interactions, Prog. NMR Spectrosc. 25 (1993) 403–480.

[2] F.X. Barre, S. Ait-Si-Ali, C. Giovannangeli, R. Luis, P. Robin, L.L. Pritchard, et al., Unambiguous demonstration of triple-helix-directed gene modification, Proc. Nat. Acad. Sci. USA 97 (2000) 3084–3088.

[3] M. Faria, C.D. Wood, M.R. White, C. Hélène, C. Giovannangeli, Transcription inhibition induced by modified triple helix-forming oligonucleotides: a quantitative assay for evaluation in cells, J. Mol. Biol. 306 (2001) 15–24.

[4] D. Praseuth, A.L. Guieysse, C. Hélène, Triple helix formation and antigene strategy for sequence-specific control of gene expression, Biochem. Biophys. Acta 1489 (1999) 181–206.

[5] H.E. Moser, P.B. Dervan, Sequence-specific cleavage of double helical DNA by triple helix formation, Science 238 (1987) 645–650.

[6] M. Mills, P.B. Arimondo, L. Lacroix, T. Garestier, H. Klump, J.L. Mergny, Chemical modification of the third strand: differential effects on purine and pyrimidine triple helix formation, Biochemistry 41 (2002) 357–366.

[7] D. Leitner, K. Weisz, Sequence-dependent stability of intramolecular DNA triple helices, J. Biomol. Struct. Dyn. 17 (2000) 993–1000.

[8] A. Houlton, M.G. Roberts, J. Silver, Studies on gold complexes of 1,1′-bis(diphenylphosphino)ferrocene, J. Organomet. Chem 418 (1991) 269–275.

[9] N. Farrel, Transition Metal Complexes as Drugs and Chemotherapeutic Agents Kluwert, Academic Publishers, Dordrecht, 1989.

[10] J.H. Murray, M.M. Harding, Organometallic anticancer agents: the effect of the central metal and halide ligands on the interaction of metallocene dihalides Cp2MX2 with nucleic acid constituents, J. Med. Chem. 37 (1984) 1936–1941.

[11] P. Köpf-Maier, F. Preiss, T. Marx, T. Klapötke, H. Köpf, Tumor inhibition by titanocene complexes: activity against sarcoma 180, Anticancer Res. 6 (1986) 33–37.

[12] G.H. Keller, M.M. Manak, DNA Probe, Stockton Press, London, 1990.

[13] T. Ihara, M. Nakayama, M. Murata, K. Nakano, M. Maeda, Gene sensor using ferrocenyl oligonucleotide, Chem. Commun. 17 (1997) 1609–1610.

[14] M. Gait, in: M. Gait (Ed.), Oligonucleotide Synthesis: a Practical Approach, IRL Press, Oxford, UK, 1984.

[15] F. Eckstein, in: F. Eckstein (Ed.), Oligonucleotides and Analogues: a Practical Approach, IRL Press, Oxford, UK, 1991.

[16] E. Bucci, L. De Napoli, G. Di Fabio, A. Messere, D. Montesarchio, A. Romanelli, et al., A new ferrocene-methyl-thymidine nucleoside: synthesis, incorporation into oligonucleotides and optical spectroscopic studies on the resulting single strand, duplex and triplex structures, Tetrahedron 55 (1999) 14435–14450.

[17] O. Mitsunobu, The use of diethyl azodicarboxylate and triphenylphosphine in synthesis and transformation of natural products, Synthesis 1 (1981) 1–28.

[18] C.R. Cantor, M.M. Warshaw, H. Shapiro, Oligonucleotide interactions. Circular dichroism studies of the conformation of deoxyoligonucleotides, Biopolymers 9 (1970) 1059–1077.

[19] G. Barone, P. Del Vecchio, D. Fessas, C. Giancola, G. Graziano, Theseus: a new software package for the handling and analysis of thermal denaturation data of biological macromolecules, J. Thermal Anal. 39 (1993) 2779–2790.

[20] E. Freire, R.L. Biltonen, Thermodynamics of transfer ribonucleic acids: the effect of sodium on the thermal unfolding of yeast tRNAPhe, Biopolymers 17 (1978) 1257–1272.

[21] K. Liu, V. Sasisekharan, H.T. Miles, Structure of Py(Pu(Py DNA triple helices. Fourier transforms of fiber-type X-ray diffraction of single crystals, Biopolymers 31 (1996) 573–589.

[22] W.P. Anderson, W.D. Edwards, M.C. Zerner, Calculated spectra of hydrated ions of the first transition-metal series, Inorg. Chem. 25 (1986) 2728–2732.

[23] A.D. Bacon, M.C. Zerner, An intermediate neglect of differential overlap theory for transition metal complexes: iron, cobalt and copper chlorides, Theor. Chim. Acta 53 (1979) 21–54.

[24] W.L. Jorgensen, J. Chandrasekhar, J.D. Madura, R.W. Impey, M.L. Klein, Comparison of simple potential functions for simulating liquid water, J. Chem. Phys. 79 (1983) 926–935.

[25] W.D. Cornell, P. Cieplak, C.I. Bayly, I.R. Gould, K.M. Merz, D.M. Ferguson, et al., A second generation force field for the simulation of proteins, nucleic acids and organic molecules, J. Am. Chem. Soc. 117 (1995) 5179–5197.

[26] J.P. Bartley, T. Brown, A.N. Lane, Solution conformation of a intramolecular DNA triple containing a non-nucleotide linker: comparison with the DNA duplex, Biochemistry 36 (1997) 14502–14511.

[27] B.L. Gaffney, P.P. Kung, C. Wang, R.A. Jones, Nitrogen-15-labeled oligodeoxynucleotides.8. Use of 15N NMR to probe Hoogsteen hydrogen bonding at guanine and adenine N7 atoms of a DNA triplex, J. Am. Chem. Soc. 117 (1995) 12281–12283.

[28] G. Manzini, L.E. Xodo, D. Gasparotto, F. Quadrifoglio, G.A. van der Marel, J.H. van Boom, Triple helix formation by oligopurine-oligopyrimidine DNA fragments: electrophoretic and thermodynamic behavior, J. Mol. Biol. 213 (1990) 833–843.

[29] R.C. Cantor, P.R. Schimmel, Biophysical Chemistry, W.H. Freeman and Company, San Francisco, USA, 1971, pp. 1145–1147.

[30] J. Santalucia, H.I. Allawi, P.A. Seneviratne, Improved nearest-neighbor parameters for predicting DNA duplex stability, Biochemistry 35 (1996) 3555–3562.

[31] V.P. Antao, D.M Gray, R.L. Ratliff, CD of six different conformational rearrangements of poly [d(A–G).d(C–T)] induced by low pH, Nucleic Acid Res. 16 (1988) 719–783.

[32] D. Leitner, W. Schroder, K. Weisz, Influence of sequence-dependent cytosine protonation and methylation on DNA triplex stability, Biochemistry 39 (2000) 5886–5892.

[33] D. Leitner, W. Schroder, K. Weisz, Direct monitoring of cytosine protonation in an intramolecular DNA triple helix, J. Am. Chem. Soc. 120 (1998) 7123–7124.

[34] J.L. Asensio, A.N. Lane, J. Dhesi, S. Bergquist, T. Brown, The contribution of cytosine protonation to the stability of a parallel DNA triple helices, J. Mol. Biol. 275 (1998) 811–822.

[35] T. Ihara, Y. Maruo, S. Takenaka, M. Takagi, Ferrocene-oligonucleotide conjugates for electrochemical probing of DNA, Nucleic Acid Res. 24 (1996) 4273–4280.